Orientation-induced enhancement in electromagnetic properties of $ZnFe_2O_4$/SiO_2/PANI core/shell/shell nanostructured disks

Cite as: AIP Advances **6**, 055908 (2016); https://doi.org/10.1063/1.4943056
Submitted: 04 November 2015 . Accepted: 03 December 2015 . Published Online: 25 February 2016

Jiaheng Wang, and Siu Wing Or

Orientation-induced enhancement in electromagnetic properties of $ZnFe_2O_4/SiO_2$/PANI core/shell/shell nanostructured disks

Jiaheng Wang and Siu Wing Or[a]
Department of Electrical Engineering, The Hong Kong Polytechnic University, Hung Hom, Kowloon, Hong Kong

(Presented 13 January 2016; received 4 November 2015; accepted 3 December 2015; published online 25 February 2016)

$ZnFe_2O_4/SiO_2$/PANI (ZSP) core/shell/shell nanostructured disks are prepared and fabricated into paraffin-bonded ZSP composite rings with random, vertical, and horizontal orientations of the easy magnetization planes of the ZSP disks in the paraffin binder in order to study the effect of directional orientation of the easy magnetization planes on their electromagnetic properties. The easy magnetization planes induced by shape anisotropy and oriented by a magnetic field in the vertically oriented ring result in a general enhancement in permeability of 7–60% in the broad UHF–Ku (0.1–18 GHz) bands, while those in the horizontally oriented ring lead to a significant enhancement of 58–1100% in the low-frequency L and S (1–4 GHz) bands, in comparison with the randomly oriented ring. The observed permeability agrees with the theoretical prediction based on the Landau–Lifshitz–Gilbert equation and the Bruggeman's effective medium theory. The horizontal and vertical arrangements of dipolar polarizations in the vertically and horizontally oriented rings give rise to 3–11% enhancement and weakening in permittivity, respectively, compared to the randomly oriented ring. The enhancement in permeability also improves and broadens the electromagnetic wave absorption in both vertically and horizontally oriented rings, especially in the L and S bands for the horizontally oriented ring. [http://dx.doi.org/10.1063/1.4943056]

I. INTRODUCTION

Electromagnetic (EM) wave absorbers based on magnetic/dielectric core/shell nanocapsules have been a main research focus to alleviate EM interference problems in recent years.[1–5] Core/shell/shell nanocapsules have been evolved more recently to broaden the absorbing bandwidth and absorber thickness range by the bandwidth-broadening effect in various core/shell/shell material phases.[6–8] In fact, the bandwidth-broadening effect is underpinned by the cooperative effect of the multidielectric polarizations in permittivity and the broadened magnetic natural resonance in permeability.[8,9] However, the deficiency in the generally weak absorption caused by the intrinsically small permeability close to unity and the inadequate EM impedance match with the relatively large permittivity has greatly impeded the nanocapsules from commercial uses, especially for the low-frequency UHF (0.3–1 GHz), L (1–2 GHz), and S (2–4 GHz) bands. The applications include commercial radios, mobile communications, satellites, global positioning system (GPS), weather and surface ship radars, etc.[1–5]

Today, magnetic cores (e.g., Ni, Fe, FeNi, Fe_3O_4, $ZnFe_2O_4$, etc.) with low-dimensional nanostructures (e.g., rod, disk, flake, etc.) have shown the ability to improve the permeability and exceed the Snoek's limit in the gigahertz frequency range because of the contribution of shape

[a]Author to whom correspondence should be addressed: electronic mail: eeswor@polyu.edu.hk

anisotropy-induced easy magnetization planes.[9–13] Moreover, Fe_3O_4 nanoflakes with their easy magnetization flake planes oriented in a preferred direction by a magnetic field have exhibited an improved permeability and an extended Snoek's limit compared to the ones without a preferred orientation.[12] Therefore, complex ferrites, which are capable of showing a higher magnetocrystalline anisotropy when doped with Ni or Zn as well as a stronger shape anisotropy when prepared as a low-dimensional nanostructure, have great potential to enhance permeability and EM wave absorption performance via a directional orientation of their easy magnetization planes.[14]

In this paper, we aim to investigate the effect of directional orientation of easy magnetization planes of magnetic nanostructured cores on the EM properties of core/shell/shell nanostructures. Accordingly, $ZnFe_2O_4/SiO_2$/PANI (denoted as ZSP) core/shell/shell nanostructured disks having a disk-shaped anisotropic $ZnFe_2O_4$ magnetic core coated by a 1st amorphous SiO_2 insulating dielectric shell and a 2nd amorphous PANI conducting dielectric shell are prepared. The ZSP disks are fabricated into three characteristic types of paraffin-bonded ZSP composite rings in the absence and presence of a dc magnetic field of controlled amplitude to randomly, vertically, and horizontally orient the easy magnetization planes of the ZSP disks during the cure of the paraffin binder. The complex relative permeability and permittivity of the ZSP composite rings are measured in the 0.1–18 GHz range, covering the UHF–Ku bands. The theoretical calculation on permeability is established by the Landau–Lifshitz–Gilbert (LLG) equation and the Bruggeman's effective medium theory (EMT) and is applied to explain the measured permeability with good agreements. The reflection loss is also determined from the measured complex relative permeability and permittivity to investigate the EM wave absorption performance.

II. EXPERIMENTAL DETAILS

The proposed ZSP core/shell/shell nanostructured disks were prepared using a three-step process described elsewhere.[9] In brief, the disk-shaped $ZnFe_2O_4$ core was synthesized using a surfactant-assisted hydrothermal method involving the co-precipitation of ZnAc of 2 mmol and $FeCl_3$ of 4 mmol in a NaOH water solution of 3.3 mol/l as well as the heating of the mixture in a Teflon-lined stainless steel autoclave at 200 °C for 4 h. The 1st SiO_2 shell was coated on the as-prepared $ZnFe_2O_4$ products using a modified stöber method in a solution containing ethanol of 10 ml, water of 3 ml, NH_4OH of 0.2 ml, and TEOS of 0.1 ml. The 2nd PANI shell was coated on the as-prepared SiO_2-coated $ZnFe_2O_4$ products using a polymerization method in a mixture of water of 50 ml, SDS of 80 mg, aniline of 8 μl, and $(NH_4)_2S_2O_8$ of 10 mg.

Three characteristic types of paraffin-bonded ZSP composite rings, all having 30 wt.% ZSP products dispersed in an EM-transparent paraffin binder, were fabricated in a nonmagnetic brass mold with an inner diameter of 3.04 mm, an outer diameter of 7 mm, and a thickness of 2 mm. These included the ones with random, vertical, and horizontal orientations of the easy magnetization planes (i.e., the two major surfaces) of the ZSP products with respect to the two major torus surfaces of the ring-shaped brass mold during the cure of the paraffin binder (upper inset of Fig. 2). For ease of description, these ZSP composite rings are denoted as the randomly, vertically, and horizontally oriented rings, respectively. The vertically and horizontally oriented rings were formed by applying a dc magnetic field of 1 T amplitude to the vertical (or perpendicular) and horizontal (or parallel) directions of the two major torus surfaces of the ring-shaped brass mold, respectively, in a temperature-controlled chamber at 60 °C for 5 h. No orientation field was required for the randomly oriented ring.

The morphology of the ZSP products was examined by a JEOL JSM-6490 scanning electron microscope (SEM). The core/shell/shell interfaces of the ZSP products were investigated using a JEM-2100F transmission electron microscope (TEM) with an operating voltage of 200 kV. The complex relative permeability ($\mu_r = \mu_r' - j\mu_r''$) and permittivity ($\varepsilon_r = \varepsilon_r' - j\varepsilon_r''$) of the ZSP composite rings were measured by a transmission/reflection coaxial cable method in the 0.1–18 GHz range using an Agilent 5244A network analyzer. The EM wave incident direction was set along the thickness direction of the ZSP composite rings. The frequency (f) dependence of reflection loss

(RL) was determined using[1,2]

$$RL = 20 \log |(Z_{in} - Z_0)/(Z_{in} + Z_0)| \quad (1)$$

where $Z_{in} = Z_0(\mu_r/\varepsilon_r)^{1/2} \tanh\left[j\,(2\pi f d/c)\,(\mu_r \varepsilon_r)^{1/2}\right]$ is the input impedance of ZSP composite ring, Z_0~377 Ω is the characteristic impedance of air, $c = 3 \times 10^8$ m/s is the velocity of light, and d is the thickness of ZSP composite ring.

III. RESULTS AND DISCUSSION

Figure 1(a) shows the SEM image of a typical ZSP product. The product has a disk-shaped morphology with a diameter of ~6 μm and a diameter-to-thickness ratio of ~3:1 (not shown). The two major surfaces of the ZSP disks are the easy magnetization planes because of shape anisotropy. Figure 1(b) illustrates the TEM image of the $ZnFe_2O_4/SiO_2$/PANI interfaces of a typical ZSP disk. The lower part with a darker contrast is the $ZnFe_2O_4$ core, while the upper part coated on the $ZnFe_2O_4$ core and with a lighter contrast is the SiO_2/PANI double-shell of ~20 nm thickness. Figure 1(c) gives the HRTEM image of the $ZnFe_2O_4/SiO_2$/PANI interfaces in Fig. 1(b). The periodic stripes of ~0.254 nm lattice plane spacing, corresponding to the (311) planes of $ZnFe_2O_4$, confirm the crystalline state of the disk-shaped $ZnFe_2O_4$ core. The 1st SiO_2 shell and the 2nd PANI shell are amorphous with thicknesses of ~5 and ~15 nm, respectively.

The symbols in Fig. 2 show the measured f dependence of μ_r' and μ_r'' for the randomly, vertically, and horizontally oriented rings. The randomly oriented ring exhibits relatively smooth μ_r' and μ_r'' spectra, except for a small magnetic natural resonance at ~1.7 GHz and a negative μ_r'' in the 13.4–18 GHz range. In particular, the occurrence of the negative μ_r'' suggests the transformation of electric energy into magnetic energy in the 2nd conducting dielectric PANI shell of the ZSP disks via the generation of magnetic fields by the electric currents of EM waves.[9] The vertically oriented ring, besides the two small magnetic natural resonances at ~4.2 and ~11.7 GHz, has an enhancement of ~7 and ~60% in μ_r' and μ_r'', respectively, throughout the whole measurement range of 0.1–18 GHz and covering the broad UHF–Ku bands, in comparison with the randomly oriented one. The horizontally oriented ring has a strong magnetic natural resonance at ~1.4 GHz, leading to a maximal enhancement of ~58 and ~1100% in μ_r' and μ_r'', respectively, in the low-frequency L (1–2 GHz) and S (2–4 GHz) bands. Moreover, μ_r' and μ_r'' are generally increased above 4 GHz due to the

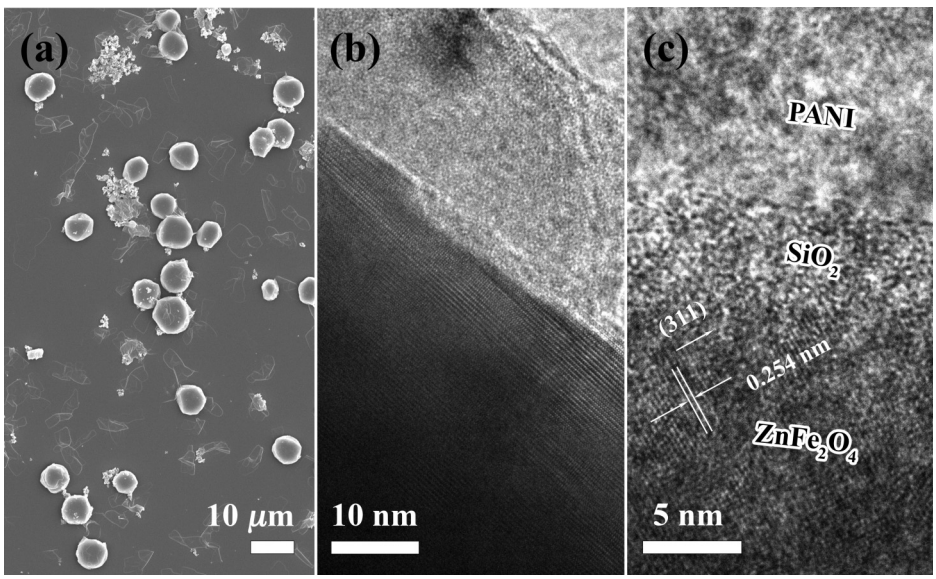

FIG. 1. (a) SEM image of a typical ZSP product. (b) TEM and (c) HRTEM images of the $ZnFe_2O_4/SiO_2$/PANI interfaces of a typical ZSP disk.

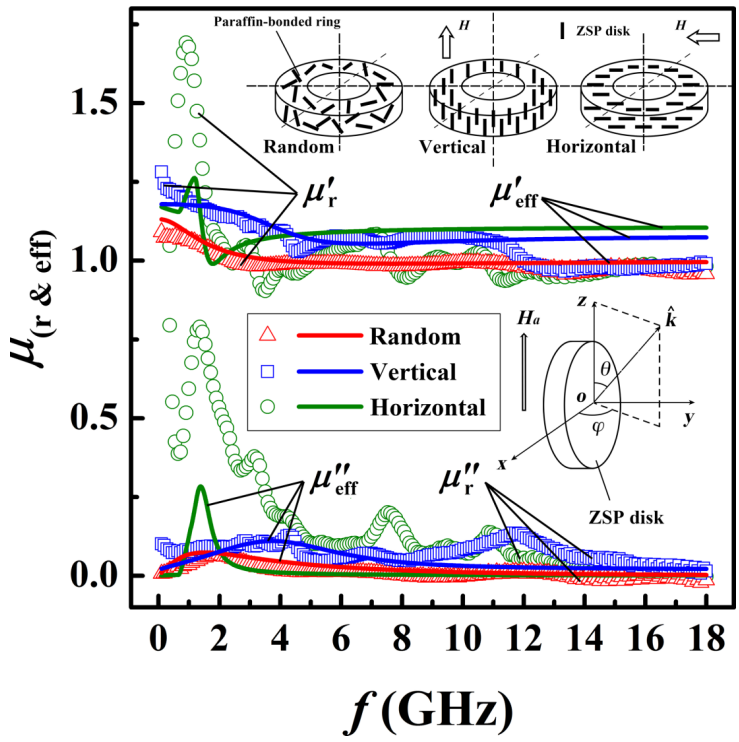

FIG. 2. Measured f dependence of μ'_r and μ''_r (symbols) and calculated f dependence of μ'_{eff} and μ''_{eff} (lines) for randomly, vertically, and horizontally oriented rings.

three higher frequency magnetic natural resonances at 3.1, 7.5, and 10.8 GHz. Comparing with the previous report on measuring the permeability tensor with an in-situ magnetic orientation field,[15] our vertically and horizontally oriented rings, owing to the pre-orientation of the easy magnetization planes of the ZSP disks by a magnetic field during the cure of the paraffin binder, do not require the in-situ magnetic orientation field in measurement and demonstrate an obvious enhancement in permeability.

In order to obtain an improved insight into the measured μ'_r and μ''_r spectra in Fig. 2, a theoretical calculation on μ_r was established by the LLG equation and the Bruggeman's EMT. As the double-shell is nonmagnetic and as thin as ~20 nm, it is ignored from the calculation and the ZSP core/shell/shell nanostructured disk is treated as a $ZnFe_2O_4$ nanostructured disk. The LLG equation can be described as[16,17]

$$\frac{d\boldsymbol{M}}{dt} = -\gamma \boldsymbol{M} \times \boldsymbol{H} + \frac{\alpha}{M_s} \boldsymbol{M} \times \frac{d\boldsymbol{M}}{dt} \tag{2}$$

where $\boldsymbol{M}$ is the magnetization, $\boldsymbol{H}$ is the effective magnetic field including applied static and dynamic fields, anisotropy field, demagnetization field, etc., γ (=2.8 MHz/Oe) is the gyromagnetic ratio, α is the damping coefficient, and M_s is the saturation magnetization. Consider a magnetic nanostructured disk having its easy magnetization planes randomly oriented with an incident EM wave ($\hat{\boldsymbol{k}}$) in the o–xyz coordinate system as shown in the lower inset of Fig. 2. Since the overall magnetization is zero, the applied static field is zero and the demagnetization field is negligible. $\boldsymbol{H}$ in Eq. (2) can be expressed by the applied dynamic field ($\boldsymbol{h}$) perpendicular to $\hat{\boldsymbol{k}}$ as well as the magnetocrystalline anisotropy field (H_a) along the easy magnetization planes of the magnetic nanostructured disk as follows:

$$\boldsymbol{H} = H_a + \boldsymbol{h} e^{j\omega t - \hat{\boldsymbol{k}} \cdot \boldsymbol{r}} = \left(h_x, -4\pi m_y + h_y, H_a + h_z\right) \tag{3a}$$

$$\boldsymbol{M} = M_0 + \boldsymbol{m} e^{j\omega t - \hat{\boldsymbol{k}} \cdot \boldsymbol{r}} = \left(m_x, m_y, M_0 + m_z\right) \tag{3b}$$

where H_a represents the only static field counted in our case, M_0 is equal to the saturation magnetization M_s, and ω is the angular frequency. Combining the Maxwell's equations with Eqs. (2) and (3), the permeability tensor can be obtained as[10–13]

$$\mu = \frac{1}{\varepsilon}\left(\frac{\delta}{j\omega}\right)^2 \begin{bmatrix} 1-\sin^2\theta\cos^2\theta & -\sin^2\theta\sin\varphi\cos\varphi & -\sin\theta\cos\theta\cos\varphi \\ -\sin^2\theta\sin\varphi\cos\varphi & 1-\sin^2\theta\cos^2\varphi & -\sin\theta\cos\theta\sin\varphi \\ -\sin\theta\cos\theta\cos\varphi & -\sin\theta\cos\theta\sin\varphi & 1-\cos^2\theta \end{bmatrix} \tag{4a}$$

$$\delta = j\omega(\mu_0\varepsilon)^{\frac{1}{2}}\left\{\frac{\left(\mu^2-\mu-\kappa^2\right)\sin^2\theta+2\mu-\left[\left(\mu^2-\mu-\kappa^2\right)^2\sin^4\theta+4\kappa^2\cos^2\theta\right]^{\frac{1}{2}}}{2\left[(\mu-1)\sin^2\theta+1\right]}\right\}^{\frac{1}{2}} \tag{4b}$$

$$\mu = 1+\frac{\omega_0'\omega_m}{\omega_0'^2-\omega^2} \tag{4c}$$

$$\kappa = \frac{-\omega\omega_m}{\omega_0'^2-\omega^2} \tag{4d}$$

where $\omega_0 = \gamma H_a$, $\omega_m = \gamma 4\pi M_s$, and $\omega_0' = \omega_0 + j\omega\alpha$.

For the randomly oriented ring, 10,000 sets of θ and φ are randomly generated to calculate an equivalent average permeability tensor using Eq. (4). For the vertically and horizontally oriented rings, $\theta = 0$ with $\varphi = \pi/2$ and $\theta = \varphi = \pi/2$ are adopted, respectively, to determine the permeability tensor because the easy magnetization planes are along the magnetic field direction as shown in the upper inset of Fig. 2. It is noted that the permeability tensor determined for the vertically oriented ring is similar to the Polder tensor reported elsewhere.[10,15,18] The eigenvalues of the permeability tensors are thus the intrinsic permeability (μ_i). Assuming the paraffin and $ZnFe_2O_4$ are both spherical (the double-shell has been neglected in the previous steps due to its nonmagnetic and thinness nature), and since the volume fraction of $ZnFe_2O_4$ (~0.07) is well below the theoretical percolation threshold of 0.33, the effective complex permeability (μ_{eff}) can be approximately calculated by Bruggeman's EMT as[17,19]

$$p\frac{\mu_i-\mu_{eff}}{\mu_i+2\mu_{eff}} + (1-p)\frac{\mu_m-\mu_{eff}}{\mu_m+2\mu_{eff}} = 0 \tag{5}$$

where p is the volume fraction of $ZnFe_2O_4$ and μ_m (=1) is the permeability of paraffin. It should be noted that although the paraffin-bonded ZSP disks are approximated by paraffin-bonded $ZnFe_2O_4$ spheres and the relatively complicated effects/interactions such as EM energy transformation, interfacial effects of core/shell/shell nanostructures, particle shape, etc. are not taken into account, the standard effective medium approximation underlying the Bruggeman's EMT is still applicable to describing the trend and natural resonances in permeability spectra.[17,20–22]

In our previous report, M_s of ZSP nanostructured disks was measured to be 24.13 emu/g.[9] According to 30 wt.% ZSP disks in our case, and using H_a = 800 Oe and α = 0.3 in the calculation, the f dependence of μ_{eff}' and μ_{eff}'' for the randomly, vertically, and horizontally oriented cases are calculated and plotted as lines in Fig. 2. It is seen that μ_{eff}' and μ_{eff}'' of the randomly oriented case agree well with the measured μ_r' and μ_r''. The good agreement is also applied to the vertically oriented case, except for the higher magnetic natural resonance at 11.7 GHz. The strong magnetic natural resonance as measured at ~1.4 GHz in the horizontally oriented ring can still be predicted by the model even though the μ_{eff}' and μ_{eff}'' values are ~60% reduced from the measured μ_r' and μ_r'' values. The discrepancy may be caused by the relatively complicated effects/interactions mentioned in the previous paragraph, including EM energy transformation, interfacial effects of core/shell/shell nanostructures, particle shape, etc.[23] Nevertheless, the model can be used to predict the shape anisotropy and directional orientation dependent transport anisotropy.[15]

Figure 3 shows the measured f dependence of ε_r' and ε_r'' for the randomly, vertically, and horizontally oriented rings. All types of rings demonstrate similar quantitative trends in the ε_r' and ε_r'' spectra. The vertically and horizontally oriented rings exhibit ~6% increment and decrement in ε_r', respectively, compared to the randomly oriented ring. In the vertically oriented ring, most of

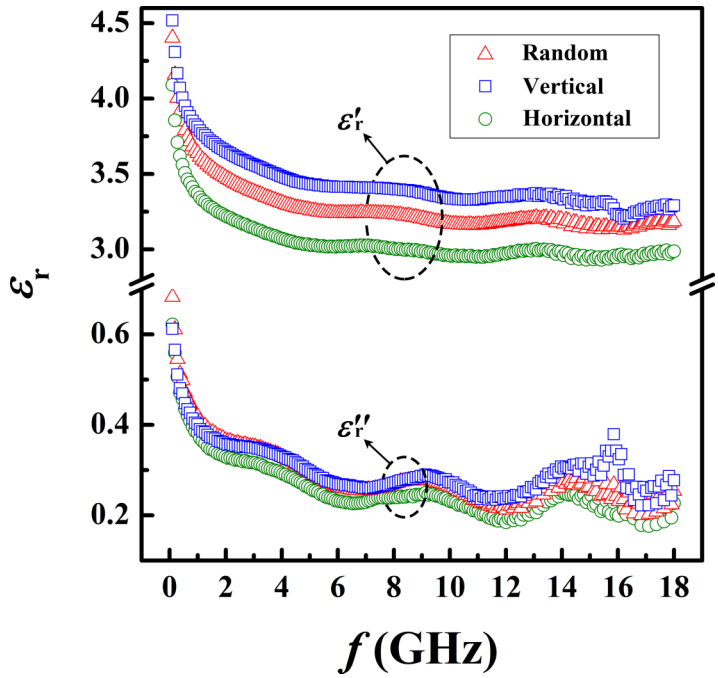

FIG. 3. Measured f dependence of ε'_r and ε''_r for randomly, vertically, and horizontally oriented rings.

the dipolar polarizations are arranged perpendicular to the easy magnetization planes of the ZSP disks (i.e., horizontal arrangement) and subject to a dynamic electric field of EM waves in the same direction so that it has a more favorable ε'_r response. The horizontally oriented ring has a vertical arrangement of dipolar polarizations and is subject to a dynamic electric field of EM waves in the orthogonal direction, so it is harder to give a ε'_r response. Similar observations are obtained for the ε''_r spectra with ~3% increment and an obvious dipolar polarization at 15.9 GHz for the vertically oriented ring as well as ~11% decrement for the horizontally oriented ring. This further infers the effect of dipolar polarization arrangement on dielectric permittivity and loss, especially for the interfaces of shape-anisotropic nanostructures.

Figure 4 displays the 2D-contour plots of the f and d dependences of RL for the randomly, vertically, and horizontally oriented rings. For the randomly oriented ring, the changes in RL basically follow a hyperbolic function of f and d, and a relatively strong absorption with RL < -5 dB is found to appear at f > 11.6 GHz (X and Ku bands) and d > 6.8mm. For the vertically oriented ring, RL is generally enhanced and broadened for f > 3 GHz (S–Ku bands) at d > 2.4mm. RL < -10 dB occurs in the 11–16 GHz range (X and Ku bands) at d > 7.6mm with a minimization

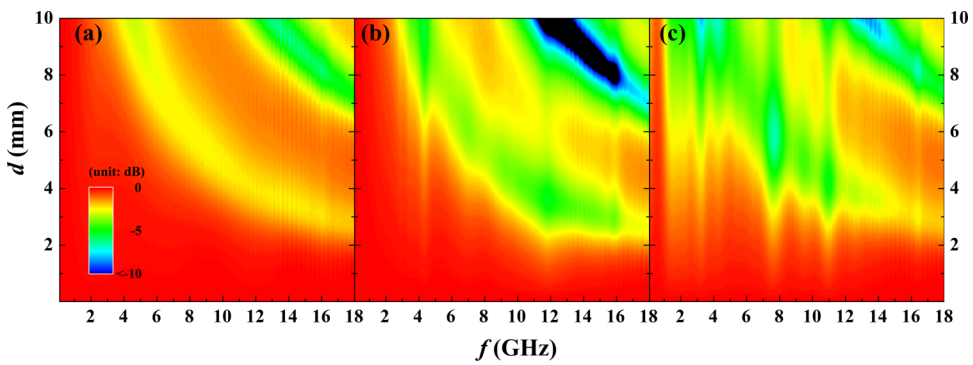

FIG. 4. 2D-contour plots of f and d dependences of RL for (a) randomly, (b) vertically, and (c) horizontally oriented rings.

of *RL* of -17.3 dB at 12.2 GHz. For the horizontally oriented ring, *RL* is significantly enhanced and broadened to cover the whole L (1–2 GHz) and S (2–4 GHz) bands as well as almost the whole C (4–8 GHz) band at $d > 7$mm owing to the permeability enhancement in these bands (Fig. 2). Strong absorptions are also extended to the X (8–12 GHz) and Ku (12–18 GHz) bands at $d = 3.5$–6.5 and 6.7–8.6 mm, respectively. The results suggest the permeability enhancement by shape anisotropy-induced, magnetic field-oriented easy magnetization planes can effectively improve the EM impedance match and hence the EM wave absorption in core/shell/shell nanostructures.

IV. CONCLUSION

We have prepared ZSP core/shell/shell nanostructured disks, fabricated paraffin-bonded ZSP composite rings with random, vertical, and horizontal orientations of the easy magnetization planes of the ZSP disks, and investigated the effect of directional orientation of the easy magnetization planes on their EM properties. We have also established a theoretical calculation for predicting permeability using LLG equation and Bruggeman's EMT. We have found that the effects of shape anisotropy and directional orientation result in two small magnetic natural resonances and a general enhancement in μ_r' and μ_r'' of ~7 and ~60%, respectively, in the broad UHF–Ku (0.1–18 GHz) bands for the vertically oriented ring. Besides, a strong magnetic natural resonance and a great enhancement in μ_r' and μ_r'' of ~58 and ~1100% are formed in the low-frequency L and S (1–4 GHz) bands for the horizontally oriented ring. The horizontal dipolar polarization arrangement in the vertically oriented ring is favorable to the ε_r' and ε_r'' responses, while the vertical dipolar polarization arrangement in the horizontally oriented ring is harder to give a response in ε_r' and ε_r'', so that their ε_r' and ε_r'' values have 3–11% increment and decrement, respectively. As a result, the EM wave absorption is enhanced and broadened in the vertically and horizontally oriented rings, especially in the L and S bands for the horizontally oriented ring.

ACKNOWLEDGEMENTS

This work was supported by the Research Grants Council of the HKSAR Government (PolyU 5236/12E) and The Hong Kong Polytechnic University (G-YK59).

[1] X. F. Zhang, X. L. Dong, H. Huang, Y. Y. Liu, W. N. Wang, X. G. Zhu, B. Lv, J. P. Lei, and C. G. Lee, Appl. Phys. Lett. **89**, 053115 (2006).
[2] X. L. Dong, X. Zhang, H. Huang, and F. Zuo, Appl. Phys. Lett. **92**, 013127 (2008).
[3] X. G. Liu, C. Feng, S. W. Or, Y. P. Sun, C. G. Jin, and W. H. Li, RSC Ad **3**, 14590 (2013).
[4] J. H. Wang, Han Wang, Jingjing Jiang, Wenjie Gong, Da Li, Qiang Zhang, Xinguo Zhao, Song Ma, and Zhidong Zhang, Cryst. Growth Des. **12**, 3499 (2012).
[5] X. G. Liu, C. Feng, S. W. Or, C. G. Jin, F. Xiao, A. L. Xia, W. H. Li, Y. P. Sun, and S. S. Zhao, Mater. Res. Bull. **48**, 3887 (2013).
[6] X. G. Liu, S. W. Or, C. M. Leung, and S. L. Ho, J. Appl. Phys. **115**, 17A507 (2014).
[7] X. G. Liu, S. W. Or, S. L. Ho, D. Y. Geng, and Z. G. Xie, J. Alloy. Compd. **509**, 9071 (2011).
[8] H. Wang, Y. Y. Dai, W. J. Gong, D. Y. Geng, S. Ma, D. Li, W. Liu, and Z. D. Zhang, Appl. Phys. Lett. **102**, 223113 (2013).
[9] J. H. Wang, S. W. Or, and C. M. Leung, J. Appl. Phys. **117**, 17A505 (2015).
[10] L. Z. Wu, J. Ding, H. B. Jiang, C. P. Neo, L. F. Chen, and C. K. Ong, J. Appl. Phys. **99**, 083905 (2006).
[11] L. Z. Wu, J. Ding, C. P. Neo, L. F. Chen, and C. K. Ong, Phys. Stat. Sol. **204**, 755 (2007).
[12] X. G. Liu, S. W. Or, C. M. Leung, and S. L. Ho, J. Appl. Phys. **113**, 17B307 (2013).
[13] W. F. Yang, L. Qiao, J. Q. Wei, Z. Q. Zhang, T. Wang, and F. S. Li, J. Appl. Phys. **107**, 033913 (2010).
[14] V. A. Potakova, V. P. Romanov, N. D. Zerev, O. I. Gromovenko, and E. V. Rubalskaya, Phys. Stat. Sol. **4**, 327 (1971).
[15] S. Mallegol, C. Brosseau, P. Queffelec, and A. Konn, Phys. Rev. B **68**, 174422 (2003).
[16] R. F. Soohoo, *Microwave Magnetics* (Harper & Row, New York, 1985).
[17] J. Youssef and C. Brosseau, Phys. Rev. B **74**, 214413 (2006).
[18] C. Brosseau, S. Mallegol, P. Queffelec, and J. Youssef, Phys. Rev. B **70**, 092401 (2004).
[19] D. Rousselle, A. Berthault, O. Acher, J. P. Bouchaud, and P. G. Zerah, J. Appl. Phys. **74**, 475 (1993).
[20] C. Brosseau and P. Talbot, IEEE Trans. Dielec. Electr. Insul. **11**, 819 (2004).
[21] C. Brosseau and P. Talbot, J. Appl. Phys. **97**, 104325 (2005).
[22] C. Brosseau, J. Youssef, P. Talbot, and A. Konn, J. Appl. Phys. **93**, 9243 (2003).
[23] J. J. Jiang, D. Li, D. Y. Geng, J. An, J. He, W. Liu, and Z. D. Zhang, Nanoscale **6**, 3967 (2014).